Journal of Mining and Metallurgy, 39 (1–2) B (2003) 3 - 22.

ELECTROCHEMISTRY OF VANADIUM(II) AND THE ELECTRODEPOSITION OF ALUMINUM-VANADIUM ALLOYS IN THE ALUMINUM CHLORIDE-1-ETHYL-3-METHYLIMIDAZOLIUM CHLORIDE MOLTEN SALT

T. Tsuda and C. L. Hussey

Department of Chemistry and Biochemistry, The University of Mississippi,
P.O. Box 1848, University, MS 38677, USA

(Received 28 December 2002; accepted 12 February 2003)

Abstract

The electrochemical behavior of vanadium(II) was examined in the 66.7-33.3 mole percent aluminum chloride-1-ethyl-3-methylimidazolium chloride molten salt containing dissolved VCl_2 at 353 K. Voltammetry experiments revealed that V(II) could be electrochemically oxidized to V(III) and V(IV). However, at slow scan rates the V(II)/V(III) electrode reaction is complicated by the rapid precipitation of V(III) as VCl_3. The reduction of V(II) occurs at potentials considerably negative of the Al(III)/Al electrode reaction, and Al-V alloys cannot be electrodeposited from this melt. However, electrodeposition experiments conducted in VCl_2-saturated melt containing the additive, 1-ethyl-3-methylimidazolium tetrafluoroborate, resulted in Al-V alloys. The vanadium content of these alloys increased with increasing cathodic current density or more negative applied potentials. X-ray analysis of Al-V alloys that were electrodeposited on a rotating copper wire substrate indicated that these alloys did not form or contain an intermetallic compound, but were non-equilibrium or metastable solid solutions. The chloride-pitting corrosion properties of these alloys were examined in aqueous NaCl by using potentiodynamic polarization techniques. Alloys containing ~10 a/o vanadium exhibited a pitting potential that was 0.3 V positive of that for pure aluminum.

Keywords: electrochemistry, vanadium, aluminium-vanadium alloys, molten salts

1. Introduction

Single-phase binary aluminum alloy films that are supersaturated with transition metal solutes exhibit enhanced resistance to chloride-induced pitting corrosion compared to pure aluminum [1]. Examples of these alloys include *Al-Cr*, *Al-Mn*, *Al-Mo*, *Al-Nb*, *Al-Ti*, *Al-W*, and *Al-Zr*. In most cases, the corrosion resistance of these alloys increases with increasing solute concentration [2], provided that the solute does not form a second-phase precipitate [3]. Because the normal equilibrium solubility of transition metals in aluminum is rarely more than about 1 % atomic fraction (a/o), it is necessary to resort to non-equilibrium alloying methods such as melt spinning, ion implantation, reactive plasma spraying, sputter deposition, and thermal evaporation to prepare these metastable alloys. Isothermal electrodeposition from chloroaluminate melts, such as those obtained by combining anhydrous aluminum chloride with sodium chloride, mixtures of sodium chloride and potassium chloride, 1-(1-butyl)pyridinium chloride (*BuPyCl*), or 1-ethyl-3-methylimidazolium chloride (*EtMeImCl*), offers another route to these non-equilibrium materials. The literature in this area has been reviewed extensively [4]. Some pertinent examples of corrosion-resistant metastable aluminum alloys that have been electrodeposited from chloroaluminate melts include *Al-Cr*, *Al-Mn*, *Al-Nb*, and *Al-Ti* [11-13].

Corrosion-resistant metastable *Al-V* alloys have been prepared by sputter deposition [2]. The chloride pitting potential of these aged alloys (about 2 years) increases monotonically with their vanadium content, rising to about 1.2 V positive of pure aluminum for alloys containing ~20 a/o vanadium. However, there is a paucity of reports describing the electrodeposition of these alloys from any solvents, including chloroaluminate molten salts. In an early investigation, Verdieck and Yentma [14] attempted to electrodeposit vanadium from the Lewis acidic 66-20-14 m/o $AlCl_3$-$NaCl$-KCl melt containing V_2O_5 or $K_2VO_2F_3$ at 429 K by using controlled current techniques, but the resulting aluminum deposits did not contain an appreciable quantity of vanadium, and the deposition potential was the same as that for aluminum. These results have been taken to indicate that the electrodeposition of vanadium from chloroaluminate molten salts takes place at potentials negative of the potential of the *Al(III)/Al* couple. Ryan et al.[15] examined the electrochemistry of several vanadium oxides and oxyhalides, including V_2O_5, Na_3VO_4, $NaVO_3$, and NH_4VO_3, in the 55.0-45.0 m/o $AlCl_3$-*EtMeImCl* melt at room temperature. However, none of these compounds could be reduced to vanadium metal or *Al-V* alloys within the electrochemical window of this solvent.

In this article, we describe the electrochemistry of vanadium solutes in the 66.7-33.3 m/o $AlCl_3$-*EtMeImCl* melt at room temperature as it pertains to the electrodeposition of *Al-V* alloys. In addition, we report the electrodeposition of *Al-V* alloys from this molten salt after it has been modified with $EtMeImBF_4$, and the chloride pitting corrosion properties of these alloys.

2. Experimental

2.1. Chemicals

Anhydrous VCl_2 (Aldrich, 95 %) was used as received. The procedures employed for the synthesis and re-crystallization of 1-ethyl-3-methylimidazolium chloride (*EtMeImCl*) were identical to those described in a previous article [16]. The re-crystallized *EtMeImCl* was melted under vacuum in a special vacuum flask for 24 h to remove traces of solvent. Anhydrous $AlCl_3$ (Fluka, puriss) was purified by triple sublimation under vacuum in a large reaction vessel. The Lewis acidic room temperature molten salt that resulted from the combination of a molar excess of $AlCl_3$ with *EtMeImCl* was purified by constant-current electrolysis between *Al* electrodes for a period of one week. Finally, the $AlCl_3$-*EtMeImCl* melt was filtered through a porosity C Pyrex glass frit (Ace Glass) and evacuated to less that 1×10^{-3} torr for 24 h to remove proton impurities [17].

The preparation of the $EtMeImBF_4$ molten salt was carried out by reacting *EtMeImCl* with NH_4BF_4 in dry acetonitrile by using a procedure roughly similar to that described by Fuller et al. [18]. For a typical reaction, 30 g (0.205 mol) of *EtMeImCl* was placed in a 500-ml flask fitted with a Pyrex glass plug and dissolved in 200 ml of acetonitrile. To this solution, a 10 % molar excess of NH_4BF_4 was added. The flask was then sealed and allowed to stir at room temperature for a week. After completion of the anion exchange process, the precipitate, which consisted of NH_4Cl and unreacted NH_4BF_4, was removed by filtration through a porosity E glass frit (Ace Glass). The molten salt solution was heated to ~343 K under vacuum (1×10^{-3} torr) for 6 hours to remove traces of water and/or acetonitrile. After a week, very small amounts of precipitate, which were not eliminated by the filtering process, were separated by decantation. The final product was colorless and transparent.

The preparation of the $EtMeImPF_6$ molten salt was carried out by reacting *EtMeImCl* with KPF_6 in dry acetonitrile [19]. In a typical synthesis, 30 g (0.205 mol) of *EtMeImCl* was placed in a 500-ml round-bottom flask fitted with a Pyrex glass plug and dissolved in 200 ml of acetonitrile. To this solution, a 10 % molar excess of KPF_6 was added. The flask was fitted with a reflux condenser, heated to 343 K, and stirred for one week. After the completion of the anion exchange process, the solution was heated to 373 K under vacuum (1×10^{-3} torr) for 6 hours to remove acetonitrile and/or water. Unreacted KPF_6 and the solid *KCl* reaction product were removed by filtration through a porosity E glass frit. The final molten salt product was nearly colorless and perfectly transparent at 373K.

2.2. Apparatus, measurements, and analysis

Electrochemical experiments were carried out in a three-electrode cell. A Pine

Instruments Teflon-sheathed *Pt* rotating disk electrode (geometrical area=0.099 cm^2) was used as the working electrode. Coils of 0.10-cm diameter *Al* wire (Alfa Aesar, 99.999 %) were used for the counter and reference electrodes. These electrodes were immersed in the melt with the same composition as the bulk melt, but were separated from the bulk melt by a porosity E glass frit. The aluminum electrodes were cleaned with a mixture of concentrated H_2SO_4, HNO_3 and H_3PO_4; rinsed with distilled H_2O; and dried under vacuum before use. All experiments were carried out in a nitrogen gas-filled glove box (VAC Atmospheres NEXUS system) with an O_2 and H_2O content <5 ppm.

Staircase voltammetry experiments were carried out with an EG&G Model 273 potentiostat/galvanostat controlled with EG&G M270 software running on a PC with a Pentium III processor. The electrodeposition of *Al-V* alloy samples was performed with an EG&G PARC Model 173 potentiostat/galvanostat equipped with a Model 179 digital coulometer plug-in module. Bulk alloy samples of approximately 10-μm thickness were deposited onto a length of 1.25-mm diameter rotating copper wire under constant-current or controlled potential conditions. These electrodeposits were washed successively with distilled water and acetone and then dried under vacuum before they were subjected to further study.

Potentiodynamic pitting corrosion measurements were carried out on bulk alloy samples at room temperature in a 0.1 mol/l aqueous solution of *NaCl* in distilled H_2O. This solution was thoroughly deaerated with nitrogen gas before each experiment. The reference electrode for these measurements was a sodium-saturated calomel electrode (SSCE), and the counter electrode was a large surface area platinum wire coil. A known length of alloy plated *Cu* wire was exposed to the *NaCl* solution by using a heat-shrink tubing mask. The sample was then scanned at 0.5 mV s^{-1} by using cyclic staircase voltammetry.

The solubility of VCl_2 in the melt was measured by using atomic absorption spectroscopy (Perkin-Elmer Model 2380). Standard methods were employed for these measurements. Surface morphology and elemental analysis of alloy samples were carried out at the University of Mississippi with a JEOL JSM-6100 scanning electron microscope, which was equipped with a Link energy-dispersive X-ray spectrometer (EDS) or with a Hitachi S-2600H scanning electron microscope system at Kyoto University, Kyoto, Japan. The *Al-V* crystal structure was probed with a Rigaku Multi Flex X-ray diffractometer in 2θ scan mode (incident angle, θ=1°) at Kyoto University. The resulting X-ray data were compared with the appropriate JCPDS card.

3. Results and Discussion

3.1. Oxidation of vanadium (II)

VCl_2 dissolved in the Lewis acidic 66.7–33.3 mole percent $AlCl_3$–*EtMeImCl* melt,

designated hereafter as "66.7 m/o melt", to produce a dark-brown-colored solution. Atomic absorption spectrophotometric analysis of the vanadium content of a saturated solution prepared at 353 K indicated that the VCl_2 solubility was 29.5 mM. Figure 1 shows cyclic staircase voltammograms recorded at a stationary platinum disk electrode as a function of scan rate in melt containing 6.8 mM VCl_2. The step size for these voltammograms was 2 mV, which is small enough to permit the analysis of these voltammograms with the conventional theories developed for linear scan voltammetry [20]. Each voltammogram shows two oxidation (A and B) and two reduction (C and D) waves. A voltammetric scan that was reversed at about 1.7 V confirms that wave C arises from the reduction of the product of the oxidation reaction that gives rise to wave A. Therefore, wave D must correspond to the reduction of the product of wave B.

To investigate waves A and C in more detail, a series of cyclic staircase voltammograms were recorded as a function of scan rate in VCl_2-saturated 66.7 m/o melt. The resulting voltammograms are shown in Fig. 2. Data derived from these voltammograms

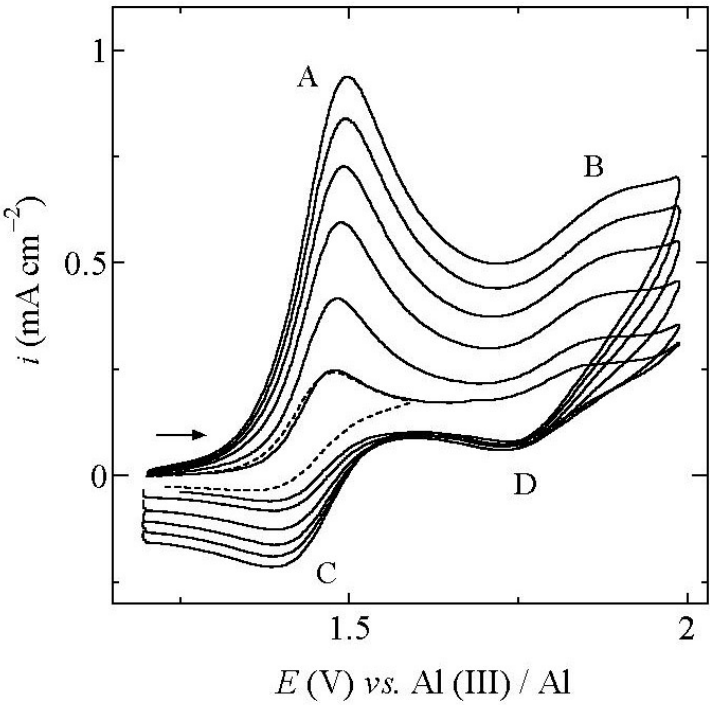

Figure 1. Cyclic staircase voltammograms recorded at a Pt stationary disk electrode in a 6.8 mM solution of VCl_2 in 66.7-33.3 m/o $AlCl_3$-EtMeImCl melt at 353 K. The scan rates were: 10, 25, 50, 75, 100, and 125 mV s^{-1}; (- - -) 10 mV s^{-1}; the step size was 2 mV.

are collected in Table 1. The data in this table show that the anodic peak current function, $i_{pa}/v^{1/2}$, is approximately independent of scan rate. However, the peak current ratio, i_{pc}/i_{pa}, which was estimated by using Nicholson's semi-empirical method [21], is less than one at slow scan rates, but increases toward one as the scan rate increases (Table 1 and Fig. 3). Thus, the electrode reaction corresponding to wave A (Fig. 1 and 2) involves an oxidation reaction with a coupled irreversible chemical step [22]. At slow scan rates, the peak potential-half peak potential separation for wave A, E_{pa}-$E_{pa/2}$ approaches the 0.067 V value, expected for a one-electron reversible electrode reaction at 353 K. However, E_{pa}-$E_{pa/2}$ increases slightly as the scan rate increases, suggesting that the electron transfer reaction may not be completely reversible. If this is the case, then both the coupled chemical step and the quasi-reversible nature of the electrode reaction may drive the positive shift in E_{pa} with increasing scan rate that is seen in Table 1 [23]. If the potential of the *Pt* electrode was scanned through wave A and held at about 1.6~1.7 V, then the electrode became covered with a violet-colored film, which was identical to VCl_3. Like $TiCl_3$, VCl_3 was found to be completely insoluble in the 66.7 m/o melt.

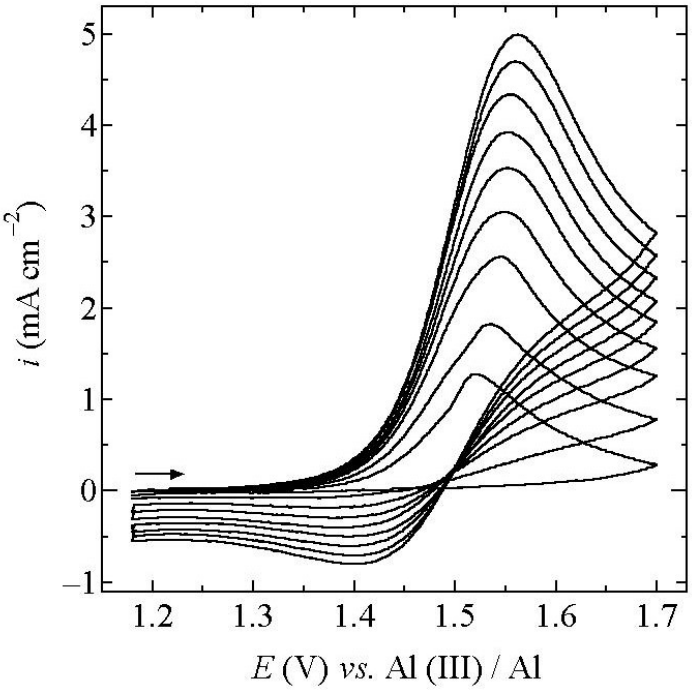

Figure 2. Cyclic staircase voltammograms recorded at a Pt stationary disk electrode in VCl_2-saturated 66.7-33.3 m/o $AlCl_3$-EtMeImCl melt at 353 K. The scan rates were: 10, 25, 50, 75, 100, 125, 150, 175, and 200 mV s^{-1}; the step size was 2 mV.

Table 1. Voltammetric data for the oxidation of V(II) at a stationary Pt electrode

ν ($V\ s^{-1}$)	$10^{-3}\ i_{pa}\nu^{1/2}$ ($A\ cm^{-2}\ V^{-1/2}\ s^{1/2}$)	$i_{pc}\ /\ i_{pa}$	E_{pa} (V)	$E_{pa/2}$ (V)	E_{pa}-$E_{pa/2}$ (V)
0.025	11.6	0.34	1.535	1.469	0.066
0.050	11.5	0.40	1.546	1.470	0.076
0.075	11.2	0.43	1.549	1.474	0.075
0.100	11.2	0.46	1.552	1.477	0.075
0.125	11.1	0.47	1.552	1.479	0.073
0.150	11.2	0.49	1.554	1.480	0.074
0.175	11.2	0.51	1.558	1.484	0.074
0.200	11.2	0.52	1.562	1.486	0.076
0.300	11.1	0.58	1.571	1.493	0.078

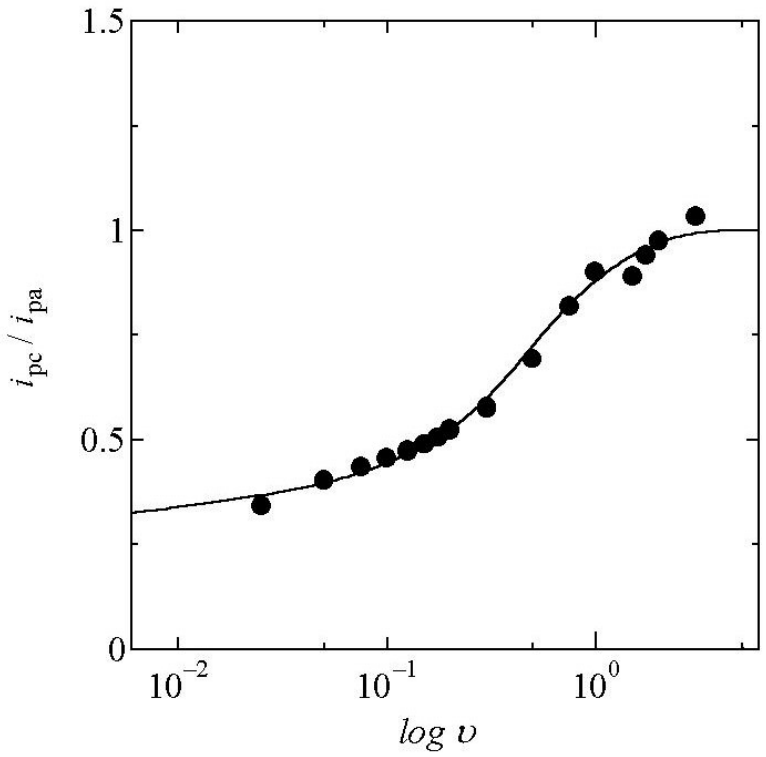

Figure 3. Plot of the ratios of the cyclic voltammetric anodic to cathodic peak currents as a function of scan rate.

Figure 1, taken together with the voltammetric results presented above, suggest that wave A arises from the one-electron quasi-reversible oxidation of solvated vanadium(II), $V(II)_{solv}$, to solvated vanadium(III), $V(III)_{solv}$, followed by precipitation of VCl_3(s) in an irreversible chemical step:

$$V(II)_{solv} \leftrightarrow V(III)_{solv} + e^- \quad (1)$$

$$V(III)_{solv} + 6AlCl_4^- \rightarrow VCl_3(s) + 3Al_2Cl_7^- \quad (2)$$

The oxidation of vanadium(II) was also examined with staircase voltammetry at a rotating *Pt* disk electrode in the same 6.8 mM solution of VCl_2 described above. The results of these experiments are shown in Fig. 4. Two oxidation waves are evident in these Pt-RDE voltammograms. These waves correspond to waves A and B in Fig. 1. Only wave A in Fig. 4 exhibits a well-defined limiting current. Furthermore, the limiting current for this wave was only observed when the scan rate was 50 mV s^{-1}, and the vanadium (II) concentration was less than about 10 mM. At slower scan rates and higher concentrations, the electrode became fouled with a passivating film of VCl_3, and no limiting current could be observed. Because of the insolubility of vanadium(III), it was not possible to obtain much useful information about waves B and D by using either voltammetric technique. However, the overall voltammetric signature for the oxidation of vanadium(II) is very similar to that for titanium(II) in this melt at this temperature [24]. That is, the voltammetric oxidation of titanium(II) results in two quasi-reversible one-electron oxidation waves; and the oxidation of titanium(II) to titanium(III) is complicated by the insolubility of $TiCl_3$. On this basis, we propose that wave B corresponds to the one electron oxidation of vanadium(III) to vanadium(IV), whereas wave D reflects the reverse of this process.

A Levich plot, i.e., a plot of the limiting current density, i_l, as a function of the square root of the electrode rotation rate, $\omega^{1/2}$, that was constructed from the data in Fig. 4 for wave A is shown in the inset of this figure. The slope of this plot was used with the Levich equation and the viscosity data given by Fannin et al. to calculate the diffusion coefficient, $D_{V(II)}$, and the Stokes-Einstein product, $D_{V(II)}\eta/T$ for $V(II)_{solv}$. The former was found to be 2.41×10^{-7} cm^2 s^{-1} at 353 K, and latter was estimated to be 3.3×10^{-11} g cm s^{-2} K^{-1}. The corresponding values for $Ti(II)_{solv}$ at this temperature in this same melt are 2.22×10^{-7} cm^2 s^{-1} and 3.1×10^{-11} g cm s^{-2} K^{-1} [24], in excellent agreement with the values for $V(II)_{solv}$. However, it should be noted that the diffusion coefficient for $Ti(II)_{solv}$ varies considerably with concentration due to the formation of a polymeric diffusing species. The value quoted here was that measured in the most dilute solution examined during the previous investigation.

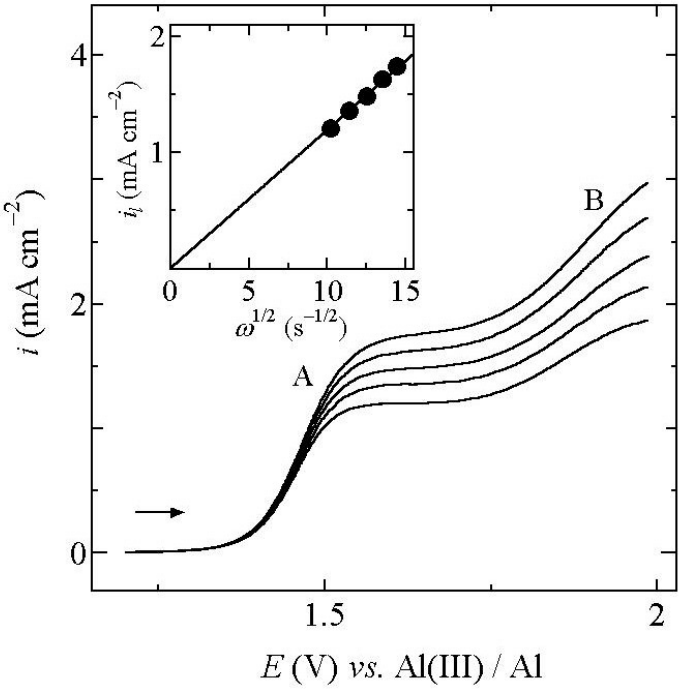

Figure 4. Staircase voltammograms recorded at a Pt-RDE in the solution described in Fig. 1. The scan rate was 50 mV s^{-1}; the step size was 2 mV; and the angular rotation frequencies were 105, 131, 157, 183, and 209 rad s^{-1}. (Inset) Relationship between the limiting current densities, i_l, and square root of the angular rotation frequencies, $\omega^{1/2}$.

3.2. Reduction of vanadium(II)

Figures 5a and 5b show cyclic staircase voltammograms recorded at a Pt-RDE in the pure 66.7 m/o melt and in the same melt after the dissolution of 29.5 mM VCl_2, respectively. In pure melt (Fig 5a), the reduction and oxidation waves centered at around 0 V correspond to the well known electrode reaction involving the electrodeposition and stripping of aluminum metal [26]:

$$4Al_2Cl_7^- + 3e^- \leftrightarrow \quad 7AlCl_4^- + Al \tag{3}$$

The dissolution of VCl_2 results in little change in the voltammetric signature for the deposition and stripping of aluminum (Fig. 5b). Thus, there is no obvious evidence for

the co-deposition of vanadium with aluminum from this melt. In order to test for the presence of vanadium in the aluminum electrodeposits, galvanostatic electrolysis experiments were performed in these solutions over the cathodic current range extending from -10 to -100 mA cm^{-2} at 353 K. A rotating Cu-wire substrate was used for all experiments. However, EDS analysis of the resulting electrodeposits revealed that they consisted of pure aluminum (Table 2). That is, no appreciable vanadium was detected in these deposits, suggesting that the equilibrium potential of the *V(II)/V* electrode reaction is negative of that for the *Al(III)/Al* reaction.

Table 2. Electrodeposited Al-V alloys

Method	$EtMeImBF_4$ (M)	Condition (V or mA cm^{-2})	Vanadium content (a/o)
Galvanostatic	0	-10 ~ -100	–
	0.23	-20 ~ -100	~0.5
	0.76	-20	1.8
		-50	6.5
		-100	8.7
Potentiostatic	0	-0.05 ~ -0.13	–
	0.76	-0.50	6.2
		-0.70	9.1

Previous research in this laboratory indicated that the fluoride-based room-temperature molten salt, $EtMeImBF_4$, may be a beneficial additive for inducing the co-deposition of vanadium with aluminum in the 66.7 m/o melt containing dissolved VCl_2. Thus, galvanostatic and potentiostatic experiments were conducted at rotating Cu-wire substrates following the introduction of this additive into the plating bath. The results of these experiments are shown in Table 2, and they indicate that this additive leads to the electrodeposition of *Al-V* alloys. However, these experiments also indicate that significant amounts of this additive must be dissolved in the plating solution before its full effect is realized. In this case, the vanadium content of the resulting *Al-V* alloys is dependent on either the deposition current density or the applied potential, depending on the plating method that was employed. Attempts to prepare *Al-V* deposits at larger cathodic current densities or at more negative potentials than those listed in the table resulted in powdery, non-adherent coatings that could not be analyzed.

In order to gain some understanding about the mode of action of the $EtMeImBF_4$ additive, cyclic staircase voltammetry experiments were conducted at a Pt-RDE in plating baths containing this ionic compound. The results of these experiments are shown in Fig. 6. A comparison of Fig. 5a with Fig. 6a indicates that adding $EtMeImBF_4$

to pure 66.7 m/o melt results in a ~200 mV negative shift in the potential at which the onset of the aluminum deposition reaction is observed. The dissolution of both $EtMeImBF_4$ and VCl_2 produces an additional negative shift and decreases the rate of the aluminum deposition process (Fig. 6b). The latter conclusion is inferred from the observation that the Pt-RDE must be scanned to ca. -0.78 V to attain approximately the same current density that is observed at -0.25 V in Fig. 6a.

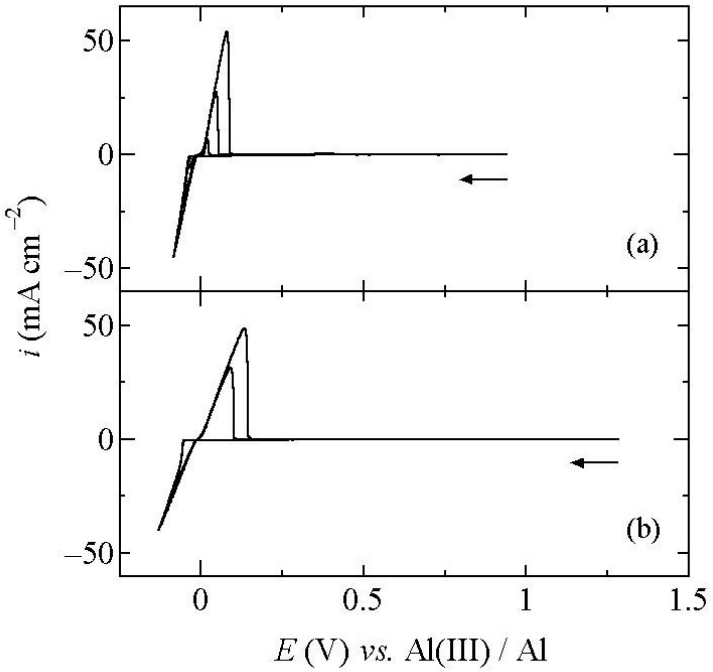

Figure 5. Staircase voltammograms recorded at a Pt-RDE in 66.7-33.3 m/o $AlCl_3$-EtMeImCl melt at 353 K: (a) pure melt, (b) melt + 29.5 mM VCl_2. The scan rate was 10 mV s^{-1}, the step size was 2 mV; and the angular frequency of rotation was 209 rad s^{-1}.

The related ionic fluoride compound, $EtMeImPF_6$, which is also a low melting salt, was tested to determine if it was a beneficial additive for inducing the co-deposition of vanadium with aluminum. To test the effects of this additive, galvanostatic and potentiostatic bulk deposition experiments similar to those described above for the $EtMeImBF_4$ additive were carried out at a rotating Cu-wire substrate over the same range of current densities and potentials. However, EDS analysis of the resulting electrodeposits indicated that no appreciable vanadium was co-deposited with aluminum from this solution, even when the concentration of the $EtMeImPF_6$ additive was identical to that used for experiments with $EtMeImBF_4$ (0.76 M).

Fig. 6c shows cyclic staircase voltammograms recorded at a Pt-RDE in 66.7 m/o melt containing both dissolved VCl_2 and $EtMeImPF_6$. Qualitatively, these voltammograms are similar to those recorded in plating baths containing VCl_2 and $EtMeImBF_4$ (Fig. 6b). However, there is one obvious difference: the addition of $EtMeImPF_6$ does not suppress the kinetics of the aluminum deposition reaction as effectively as does $EtMeImBF_4$. That is, the negative shift in the potential for the onset of the aluminum deposition reaction is smaller in plating baths containing the former additive compared to baths containing the latter compound.

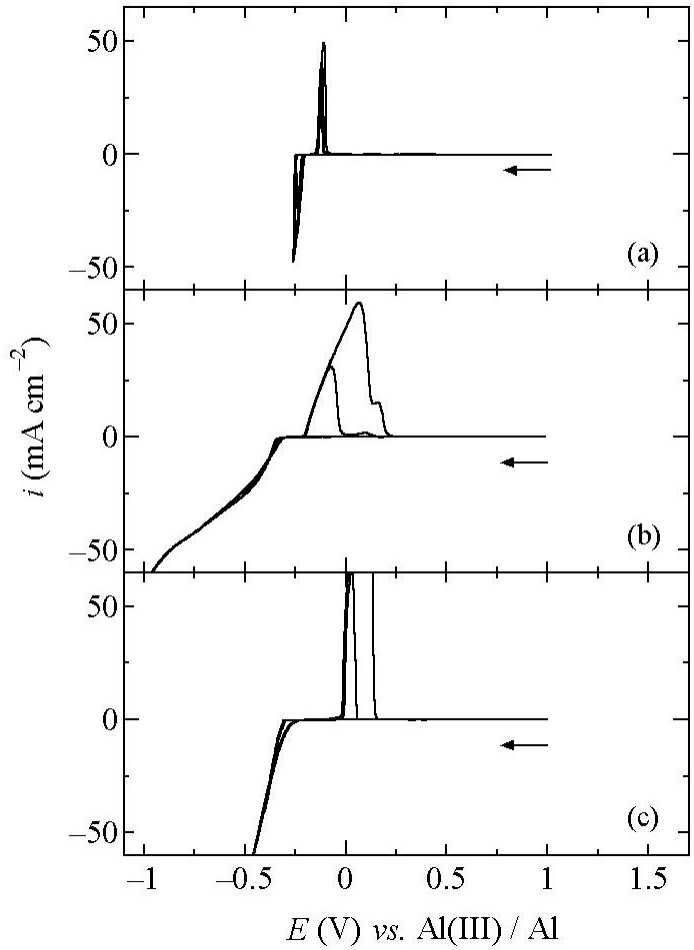

Figure 6. Staircase voltammograms recorded at a Pt-RDE in 66.7-33.3 m/o $AlCl_3$-EtMeImCl melt at 353 K: (a) melt + 0.76 M $EtMeImBF_4$, (b) the solution in Fig. 5b + 0.76 M $EtMeImBF_4$, and (c) the solution in Fig. 5b + 0.76 M $EtMeImPF_6$. The scan rate was 10 mV s^{-1}, the step size was 2 mV; and the angular frequency of rotation was 209 rad s^{-1}.

The forgoing voltammetric experiments suggest that the mode of action of the $EtMeImBF_4$ additive is to facilitate the electrodeposition of vanadium at the expense of the electrodeposition of aluminum. Because the *V(II)/V* electrode reaction lies negative of *Al(III)/Al*, this additive allows more negative potentials to be accessed before the onset of aluminum deposition. At the same time, it greatly suppresses the rate of the aluminum deposition reaction. Thus, for a given applied potential or current density, the partial current density for vanadium deposition would be a larger fraction of the total current density, enhancing the amount of vanadium in the electrodeposits. In view of these results, it is curious that the addition of $EtMeImPF_6$ to plating baths containing dissolved VCl_2 does not lead to similar results. Although both BF_4^- and PF_6^- are often thought to be relatively inert, non-coordinating anions, the former may not be as inert as supposed when added to the strongly Lewis acidic 66.7 m/o melt. For example, the conjugate acid of the latter species, PF_5, is a stronger Lewis acid than $AlCl_3$, whereas BF_3 is a weaker Lewis acid than $AlCl_3$ [27]. Thus, the beneficial effects of the $EtMeImBF_4$ additive that are reported herein may be due to alteration of the melt chemistry and/or anionic speciation as a result of a reaction between the Lewis base, BF_4^-, and the principal Lewis acidic species in the melt, $Al_2Cl_7^-$. The fact that a relatively high concentration of $EtMeImBF_4$ is needed to effect the electrodeposition of *Al-V* alloy tends to support an equilibrium reaction between BF_4^- and $Al_2Cl_7^-$. Such reactions either do not take place or are less extensive for the less basic PF_6^- anion. However, an investigation of the chemistry of BF_4^- and PF_6^- in the $AlCl_3$-*EtMeImCl* melt using techniques such as ^{27}Al NMR and Raman spectroscopy is needed in order to fully understand why and how BF_4^- facilitates the electrodeposition of *Al-V* alloys, whereas PF_6^- does not. Unfortunately, such an investigation is outside the scope of this study.

3.3. Characterization of Al-V electrodeposits

Figures 7 and 8 show SEM photographs illustrating the surface morphology of bulk *Al-V* samples electrodeposited on Cu-wire substrates using galvanostatic and potentiostatic techniques as described above. In all cases, the *Al-V* alloys appear to nucleate along the striations of the drawn copper wire surface. The surface morphology is clearly dependent on the applied current density. For example, the sample prepared at -20 mA cm^{-2} (Fig. 7a), which is the lowest current density that was investigated, shows a fine, leaf-like structure. As the cathodic current density is increased to -50 mA cm^{-2}, the resulting electrodeposit assumes a more compact, nodular structure (Fig. 7b), whereas those prepared at the highest practical current density, -100 mA cm^{-2}, are by comparison, relatively smooth and compact (Fig. 7c). Thus, grain refinement is apparently driven by the incorporation of vanadium into the aluminum deposit because an increase in the

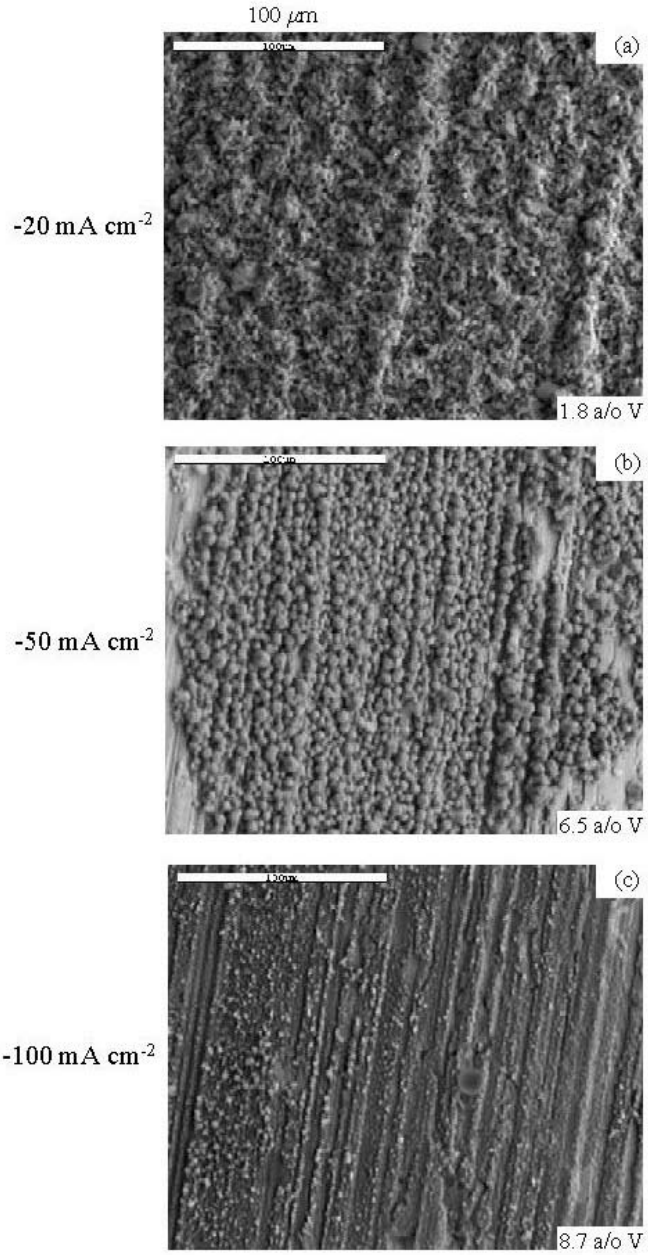

Figure 7. SEM images of Al-V alloys electrodeposited at 353 K from 66.7-33.3 m/o $AlCl_3$-EtMeImCl melt containing 29.5 mM VCl_2 and 0.76 M $EtMeImBF_4$ by using galvanostatic techniques.

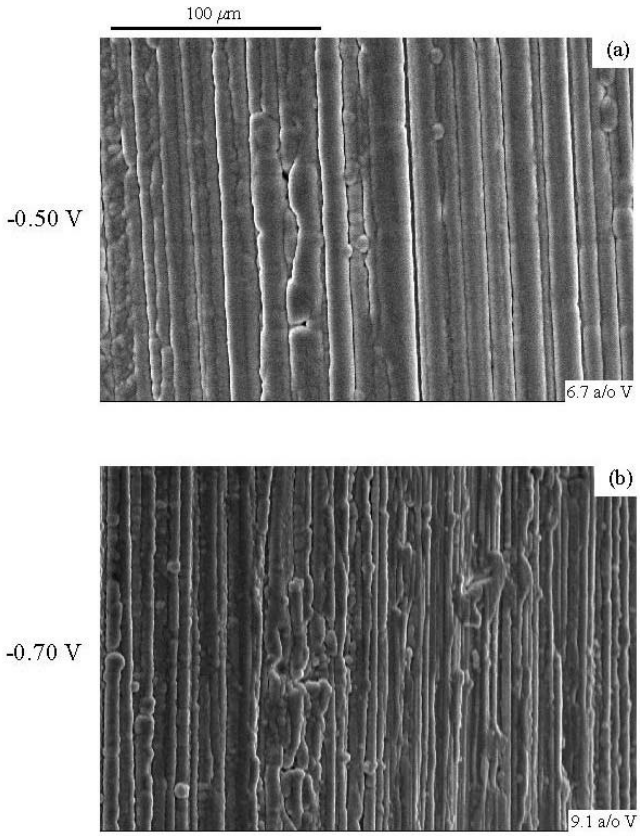

Figure 8. SEM images of Al-V alloys electrodeposited at 353 K from 66.7-33.3 m/o $AlCl_3$-EtMeImCl melt containing 29.5 mM VCl_2 and 0.76 M $EtMeImBF_4$ by using potentiostatic techniques.

deposition current density would ordinarily lead to an increase in grain size. Similarly, both of the samples that resulted from potentiostatic electrodeposition experiments exhibited a reasonably smooth, compact surface morphology (Figs. 8a and 8b). EDS elemental compositional maps were prepared for the *Al-V* electrodeposit with the highest vanadium content (Fig. 8b) and are shown in Fig. 9. These maps reveal a very uniform microdistribution of aluminum and vanadium in this sample. EDS analysis of the various *Al-V* alloy samples prepared during the course of this study indicated that all were free from chloride contamination.

Figure 10 shows an XRD pattern collected for the as deposited *Al-V* sample containing 9.1 a/o *V*. All XRD peaks were identified either with aluminum or with the copper substrate. Reflections for α-$Al_{10}V$, an intermetallic compound that might be

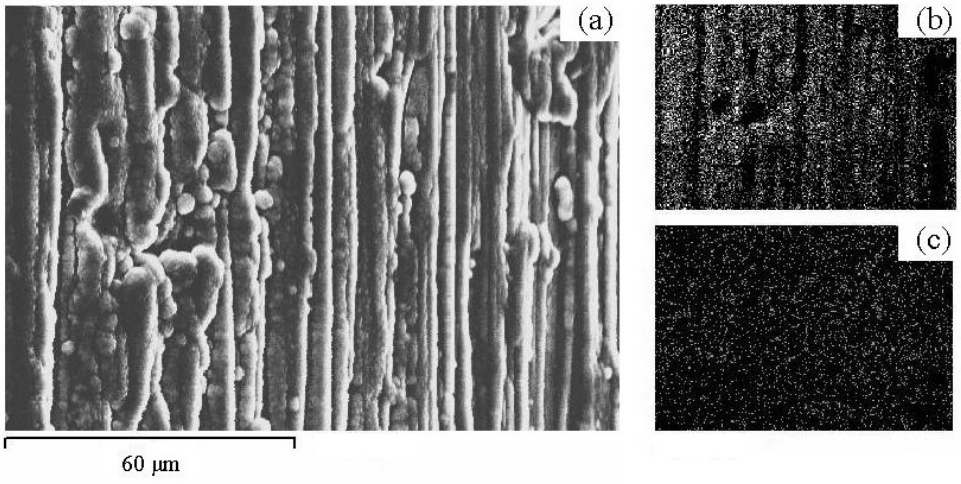

Figure 9. SEM and EDS images of the $Al_{90.9}V_{9.1}$ alloy shown in Fig. 8b: (a) SEM image, (b) aluminum EDS map, and (c) vanadium EDS map.

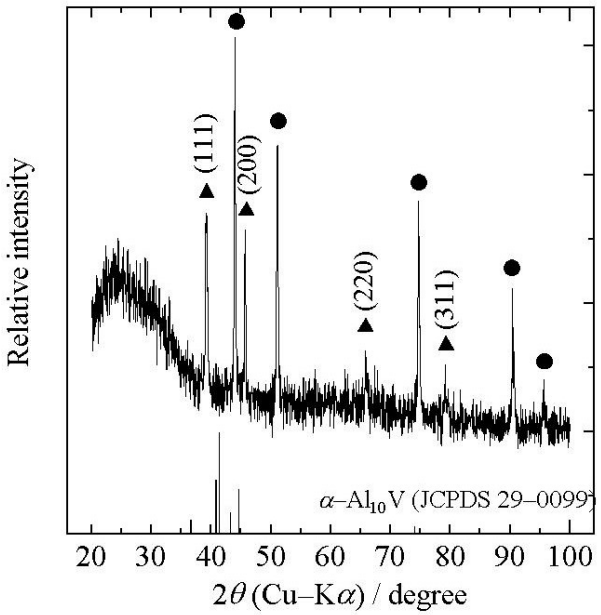

Figure 10. X-ray diffraction pattern of the $Al_{90.9}V_{9.1}$ alloy shown in Fig. 8b: reflections attributed to (●)copper and (▲) aluminum. The diffraction pattern for α-$Al_{10}V$ (JCPDS Card # 29-0099) is shown for comparison.

expected based on the *Al/V* elemental ratio of this deposit, are shown at the bottom of this figure for comparison. The lack of any reflections that can be assigned to discrete *Al-V* intermetallic compounds suggests that vanadium has alloyed substitutionally with aluminum in this deposit to form a non-equilibrium or metastable solid solution. Similar results were found for *Al-Ti* alloys prepared in the Lewis acidic $AlCl_3$-*EtMeImCl* melt containing dissolved $TiCl_2$ [24].

3.4. Pitting potential measurements

The corrosion resistance of the *Al-V* alloys described in Table 2 was investigated by recording potentiodynamic anodic polarization curves in N_2-saturated aqueous 0.1 M *NaCl*. These polarization curves are shown in Fig. 11. As noted for *Al-Mn* alloys examined under similar conditions [8], *Al-V* alloys display a stable passive region characterized by a very small potential-independent current followed by a sudden rise in current at the pitting potential. This same result was also noted for electrodeposited *Al-Ti* alloys [24].

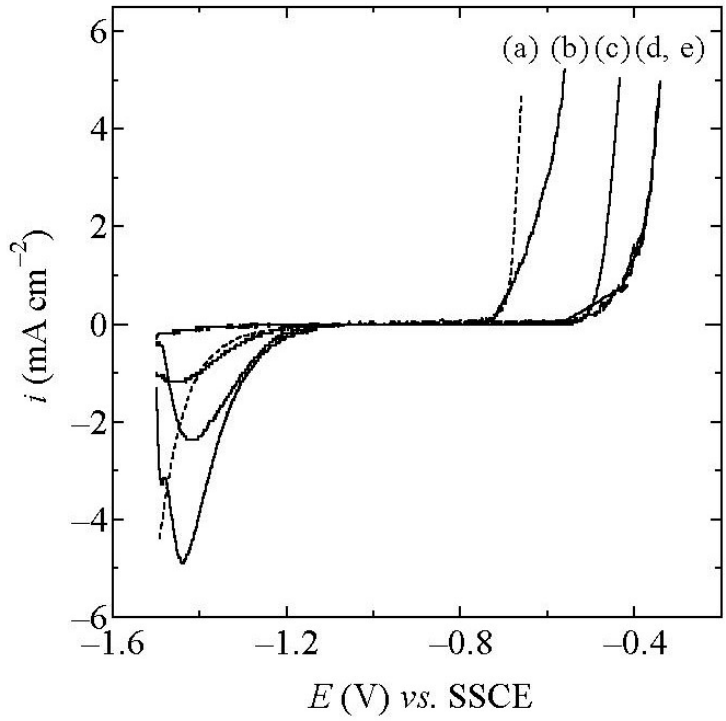

Figure 11. Potentiodynamic polarization curves for Al and Al-V alloys recorded in N_2-saturated aqueous 0.1 M-NaCl at 298 K: (a) Al (99.999 %), (b) $Al_{99.5}V_{0.5}$, (c) $Al_{98.2}V_{1.8}$, (d) $Al_{93.8}V_{6.2}$, and (e) $Al_{90.9}$ $V_{9.1}$.

The variation of the *Al-V* pitting potential with alloy composition is shown in Fig. 12. The addition of ~10 a/o vanadium increases the pitting potential of the alloy by about +0.3 V. This increase is only about 50 % that seen for *Al-V* alloys with the same composition that were prepared by sputter deposition [2], but it is comparable to the improvement in pitting potential seen for *Al-Ti* alloys containing ~10 a/o titanium that were prepared in this same molten salt by using similar techniques. One possible explanation for the difference in the pitting potentials of the electrodeposited and sputter-deposited *Al-V* alloys is the fact that the latter were aged for about 2 years before they were tested, whereas the pitting potentials of the former were measured within a few weeks of their preparation.

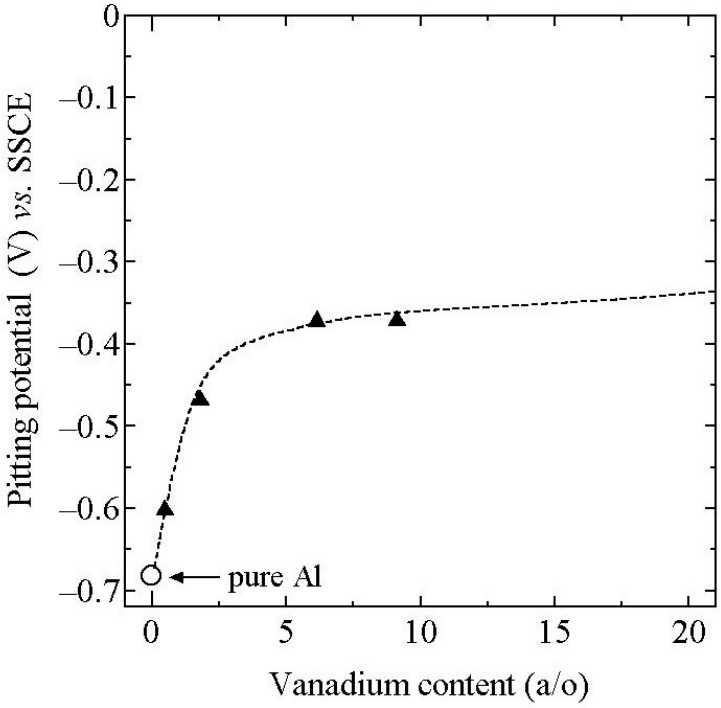

Figure 12. Pitting potentials as a function of alloy composition for the electrode posited Al-V alloys in Fig. 11 and Table 2.

4. Conclusions

Al-V alloys containing ~10 a/o vanadium can be electrodeposited from the 66.7-33.3 m/o $AlCl_3$-*EtMeImCl* molten salt containing dissolved VCl_2, provided that high concentrations of the additive, $EtMeImBF_4$, are present in the plating solution. However, the

addition of similar amounts of the related fluoride salt, $EtMeImPF_6$, to the plating bath does not lead to the co-deposition of vanadium with aluminum. *Al-V* alloys that were electrodeposited from the $AlCl_3$-*EtMeImCl* melt were dense and compact. They appear to be non-equilibrium or metastable solid solutions in which vanadium has substituted into the aluminum lattice. The chloride pitting potential of the $Al_{90.9}V_{9.1}$ alloy was about +0.3 V greater than that of pure aluminum and was comparable to the pitting potential of the $Al_{90}Ti_{10}$ alloy that was electrodeposited from 66.7-33.3 m/o $AlCl_3$-*EtMeImCl* containing $TiCl_2$. However, the pitting potential of the electrodeposited $Al_{90.9}V_{9.1}$ alloy sample prepared during this investigation was inferior to that of aged samples of similar composition that were prepared by sputter deposition.

Acknowledgment

The authors would like to express their appreciation to Prof. Yasuhiko Ito, Dr. Toshiyuki Nohira, and Dr. Takahisa Iida of Kyoto University for their assistance. This research was supported by the U.S. Air Force Office of Scientific Research, Grant No. F49620-00-1-0123.

References

1. K. Hashimoto, in Uhlig's Corrosion Handbook (R.W. Revie), John Wiley & Sons, Inc., New York, 2000, p. 929.
2. G.S. Frankel, R.C. Newman, C.V. Jahnes, M.A. Russak, J. Electrochem. Soc., 140 (1993) 2192.
3. C.C. Streinz, P.J. Moran, J.W. Wagner, J. Kruger, J. Electrochem. Soc., 141 (1994) 1132.
4. G.R. Stafford, C.L. Hussey, Advances in Electrochemical Science and Engineering, Wiley-VCH Verlag GmbH, Weinheim, 2002, p. 275.
5. T.P. Moffat, J. Electrochem. Soc., 141 (1994) L115.
6. M.R. Ali, A. Nishikata, T. Tsuru, Electrochim. Acta, 42 (1997) 2347.
7. L.W. Austin, M.G. Vucich, E.J. Smith, Electrochem. Tech., 1 (1963) 267.
8. T.P. Moffat, G.R. Stafford, D.E. Hall, J. Electrochem. Soc., 140 (1993) 2779.
9. G.R. Stafford, G.M. Haarberg, Plasmas & Ions, 1 (1999) 35.
10. N. Koura, T. Kato, E. Yumoto, J. Surf. Finish. Soc. Jpn., 45 (1994) 805.
11. T. Takenaka, M. Kawakami, Int. J. Mater. and Product Tech., 2 (2001) 500.
12. G.R. Stafford, T.P. Moffat, J. Electrochem. Soc., 142 (1995) 3288.
13. G.R. Stafford, J. Electrochem. Soc., 141 (1994) 245.
14. R.G. Verdieck, L.F. Yntema, J. Phys. Chem., 48 (1944) 268.
15. D.M. Ryan, T.L. Riechel, T. Welton, J. Electrochem. Soc., 149 (2002) A371.
16. J.S. Wilkes, J.A. Levisky, R.A. Wilson, Inorg. Chem., 21 (1982) 1263.

17. M.A.M. Noel, P.C. Trulove, R.A. Osteryoung, Anal. Chem., 63 (1991) 2892.
18. J. Fuller, R.T. Carlin, R.A. Osteryoung, J. Electrochem. Soc., 144 (1997) 3881.
19. K.R. Seddon, A. Stark, M.J. Torres, Pure Appl. Chem., 72 (2000) 2275.
20. A.J. Bard, L.R. Faulkner, Electrochemical Methods: Fundamentals and Applications, John Wiley & Sons, New York, 2001.
21. R.S. Nicholson, Anal. Chem., 37 (1965) 1406.
22. R.S. Nicholson, I. Shain, Anal. Chem., 36 (1964) 706.
23. D.H. Evans, J. Phys. Chem., 76 (1972) 1160.
24. T. Tsuda, C.L. Hussey, G.R. Stafford, J.E. Bonevich, J. Electrochem. Soc., 150 (2003) C234.
25. A.A. Fannin, Jr., L.A. King, J.A. Levisky, J.S. Wilkes, J. Phys. Chem., 88 (1984) 2609.
26. J. Robinson, R.A. Osteryoung, J. Electrochem. Soc., 127 (1980) 122.
27. D. Cook, Can J. Chem., 41 (1963) 522.